Supporting information

Releavling the Effect of Electrochemical Promotion on FeNC Catalyst for Electro-assisted NH_3-SCR

Xinying Liu,[ab] Qingling Liu,*[ab] Yan Zhang,[ab] Yuankai Shao,[c] Bingjie Zhou,[c] Zhenguo Li,*[c] Caixia Liu,*[ab] Xiaona Yan,[d] and Bin Shen[d]

[a]School of Environmental Science and Engineering, Tianjin University, Tianjin 300350, China

[b]State Key Laboratory of Engines, Tianjin University, Tianjin 300350, China

[c]National Engineering Laboratory for Mobile Source Emission Control Technology, China Automotive Technology & Research Center Co., Ltd., Tianjin 300300, P. R.China

[d]China Internal Combustion Engine Industry Association, Beijing, 100825, China.

Table of contents

1. Experimental Section

1.1 Catalyst Preparation

Synthesis of Fe_xN_yC. Firstly, the CNTs were refluxed in concentrated HNO_3 at 120 °C for 6 h, washed with deionized water, and then vacuum dried at 60 °C for 12 h. 0.6 g of treated CNTs , 2.14 g $Fe(acac)_3$, and 5.04 g $C_3H_6N_6$ were mixed in a planetary ball mill and milled at 500 rpm for 3 h. Then the mixture was calcined at 700 °C for 2 h in N_2 and at 300 °C for 2 h in air. According to the proportion of $Fe(acac)_3$ and $C_3H_6N_6$, the catalyst was named as Fe_xN_yC. $Fe_3CNT/N_{1.5}CNT$ was prepared by the same method as that for Fe_xN_yC, except for adding $C_3H_6N_6/Fe(acac)_3$, [1]

Synthesis of Fe_3CNT. 0.6 g of treated CNTs and 2.14 g $Fe(acac)_3$ were mixed in a planetary ball mill and milled at 500 rpm for 3 h. Then the mixture was calcined at 700 ℃ for 2 h in N_2 and at 300 ℃ for 2 h in air.

Synthesis of $N_{1.5}CNT$. 0.6 g of treated CNTs and 5.04 g $C_3H_6N_6$ were mixed in a planetary ball mill and milled at 500 rpm for 3 h. Then the mixture was calcined at 700 ℃ for 2 h in N_2 and at 300 ℃ for 2 h in air.

Synthesis of $Fe_3N_{1.5}C$-S. 1 ml $Fe_3N_{1.5}C$ were treated in the flow of 200 ppm SO_2 and 10 % H_2O balanced with air in a tube furnace with a gas hourly space velocity (GHSV) of 36,000 h^{-1} at 150 °C for 10 h.

1.2 Catalytic Activity Evaluation

The catalyst activity was assessed utilizing a specialized fixed-bed reactor, as depicted in Fig. 1. The reactor consisted of a dedicated quartz tube housing, a constant power supply unit, a temperature monitoring system, an electric heating furnace, and a gas distribution apparatus. The catalyst, in a quantity of 0.7 ml and ranging from 40-60 mesh, was loaded between two sintered copper sheets within the quartz tube, which possessed an inner diameter of 12 mm. These two copper sheets were each in direct contact with a copper rod and a copper wire, serving as the positive and negative electrodes, respectively, and powered by the constant power supply. A K-type thermocouple, inserted through a small aperture in the quartz tube wall, was positioned between the two copper plates to monitor the catalyst temperature. The reactant feed gas composition consisted of 500 ppm NO, 500 ppm NH_3, 5 vol% O_2, and N_2 as the balance gas, with a total flow rate of 420 mL/min, corresponding to a gas hourly space velocity (GHSV) of 36000 h^{-1}. The reaction was conducted within the temperature range of 50 to 200°C, and data collection commenced once the reaction attained a stable state. The NO_x conversion and N_2 selectivity were determined using Eqs. (1-2):

$$NO_X\,conversion = \frac{C_{NO_X(in)} - C_{NO_X(out)}}{C_{NO_X(in)}} \times 100\% \tag{1}$$

$$NO_X\,selectivity = \left(1 - \frac{2C_{N_2O(out)}}{C_{NO_X(in)} + C_{NH_3(in)} - C_{NO_X(out)} - C_{NH_3(out)}}\right) \times 100\% \tag{2}$$

1.3 Characterization Methods

Powder X-ray diffraction (XRD) measurements were conducted at 40 mA and 40kV using Cu K α radiation on a Rigaku Smart lab-SE XRD diffractometer. The 2θ data from 5° to 80°were recorded with a step size of 0.05° at 2°·min^{-1}.

High-resolution transmission electron microscopy (HR-TEM) micrographs were conducted on a JEOL JEM-F200 electron microscope equipped with a field emission source operating at 200 kV. The elemental local, mapping and line-scanning analyses were collected by energy dispersive spectroscopy (EDS) using a JED-2300T electron microscope.

A Micromeritics ASAP 2460 automatic adsorption instrument was used to measure the Brunauer–Emmett-Teller (BET) surface area at 77 K. Before N_2 physisorption, the samples were outgassed for 4 h at 210°C. The specific surface area was calculated using the Brunauer-Emmett-Teller (BET) method. The micropore volume was calculated using the t-plot method and the corresponding pore size distribution was calculated using Horvath + Saito Foley method. Both the mesopore volume and corresponding pore size distribution were calculated using the Barrett-Joyner-Halenda (BJH) method.

A Micromeritics AutoChem 2920 instrument was applied to perform temperature-programmed reduction with NH_3 (NH_3-TPD) experiments. Before each test, 100 mg of the catalyst was purged by a flowing N_2 (50 mL·min^{-1}) at 500°C for 30 min, and then the sample was cooled down to 100°C. Subsequently, ammonia was adsorbed at this temperature for 30 min to ensure the sufficient adsorption of NH_3. Before desorption, the sample was purged by a flowing He stream at

100°C for 1 h to remove excessive and physically adsorbed NH_3. Finally, the sample was heated from 100 to 700°C at a rate of 15 $°C·min^{-1}$ in a pure N_2 (50 $mL·min^{-1}$) flow and the desorption pattern was recorded.

Temperature programmed reduction of H_2 (H_2-TPR) experiment was conducted on a Micromeritics AutoChem 2920 chemisorption analyzer. Before reduction, 100 mg of the catalyst was purged by a flowing N_2 (50 $mL·min^{-1}$) at 500°C for 1 h, and then the sample was cooled down to 80°C in an N_2 flow. The temperature-programmed reduction process was performed in flow of 10% H_2/Ar (50 $mL·min^{-1}$) up to 900°C at a rate of 15 $°C·min^{-1}$.

The Raman spectra were measured on a Thermo Fisher DXR Raman microscope. The 532 nm line was used as the excitation source.

In-situ diffuse reflectance infrared Fourier transform spectroscopy (in-situ DRIFTS) experiments were carried out on a FTIR spectrometer (Nicolet iS50) equipped with a MCT detector and KBr window. All characterizations are dehydrated catalysts in this work, and the dehydration conditions were calcined at 300°C for 2 h in a muffle furnace. All DRIFTS spectra were recorded by accumulating 64 scans with a resolution of 4 cm^{-1}.

The SCR kinetics tests over the catalysts were performed in the same fixed-bed reactor. To eliminate the effects of internal and external diffusion, the GHSV was increased to 900000 h^{-1}. The kinetics data were recorded from 50 to 200°C with the NO_x conversion less than 20%.

2. Supporting Figures

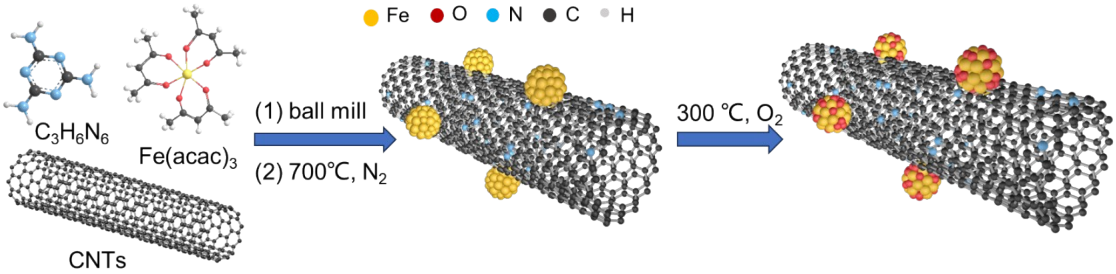

Figure S1 Schematic diagram of the process of preparing Fe_xN_yC catalyst by ball milling-pyrolysis method

The preparation process of Fe_xN_yC is shown in Fig. S1. Firstly, Fe(acac)$_3$, melamine and acid-treated carbon nanotubes were subjected to high-speed ball milling to fully integrate Fe(acac)$_3$ and melamine onto the surface of CNTs. Then, they were calcined in a 700 °C N_2 for 2h, so that melamine and Fe(acac)$_3$ were pyrolyzed to obtain N-doped CNTs loaded with iron nanoclusters. Then, the iron nanoclusters were oxidized and the unstable carbon components were burned by calcination in a 300 °C O_2, and finally Fe_xN_yC was obtained.[1]

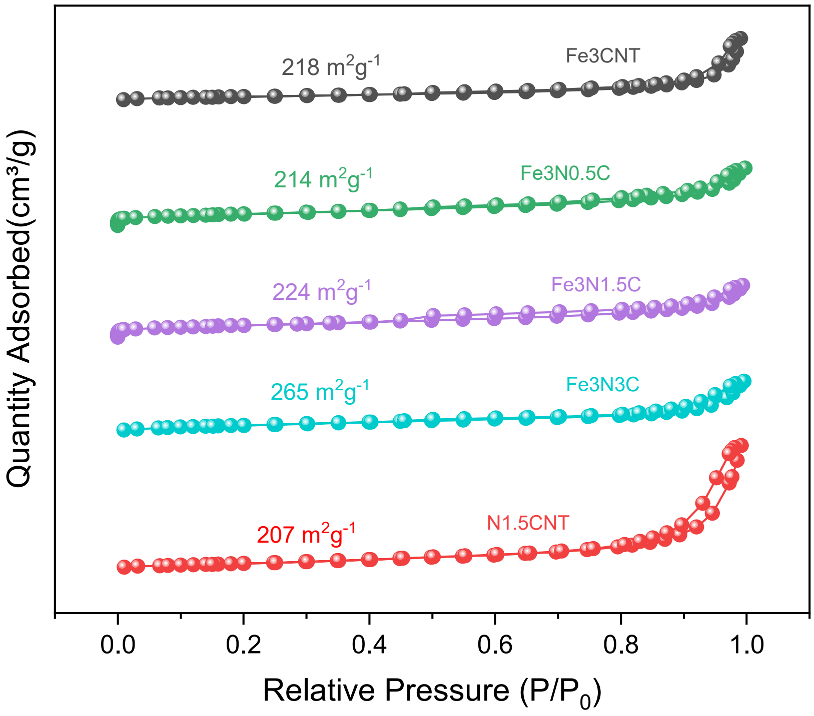

Figure S2 N_2 adsorption－desorption isotherms of Fe_3N_yC, Fe_3CNT and $N_{1.5}CNT$ catalysts

N_2 physical adsorption (Figure S2) shows that NCNTs provide a large specific surface area as a carrier, which is conducive to the adsorption of more active components and reactants. After loading Fe and increasing N precursors, the specific surface area and pore volume of the catalyst will increase slightly. The slight increase in surface area should be attributed to the incorporation of N to make the iron oxide clusters better dispersed and form more intergranular pores.

Table S1 Surface area and pore structure parameters of Fe_3N_yC, Fe_3CNT and $N_{1.5}CNT$ catalysts.

Samples	S_{BET} (m^2g^{-1})	Pore volume(cm^3 g^{-1})	Pore size (nm)
Fe_3CNT	177.41	0.057	1.274
$Fe_3N_{0.5}C$	214.22	0.060	1.102
$Fe_3N_{1.5}C$	223.88	0.065	1.134
Fe_3N_3C	264.64	0.079	1.183

$N_{1.5}$CNT	207.27	0.062	1.178

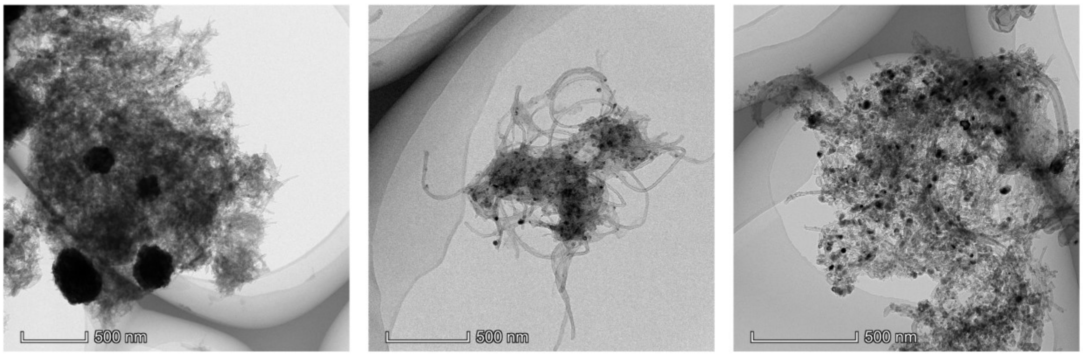

Figure S3 Transmission electron microscopy (TEM) image of Fe_3CNT, $Fe_3N_{1.5}C$, and Fe_3N_3C.

The TEM images of Fe_3CNT, $Fe_3N_{1.5}C$ and Fe_3N_3C (Figure S3) also show that the particle size of iron oxide nanoparticles on the catalyst is significantly reduced after nitrogen doping, which means that N doping can effectively improve the dispersion of iron oxide nanoparticles.

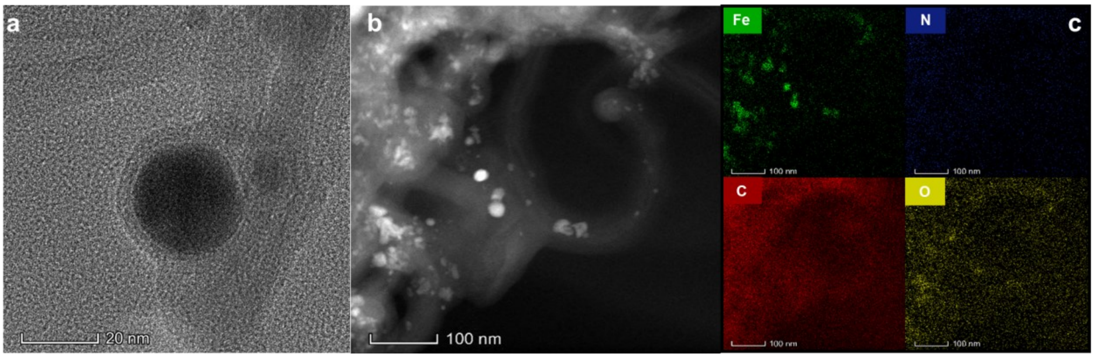

Figure S4 NO_x conversion of the catalysts under TRA and ELEC at 100 °C.

The HRTEM image (Figure S4a) shows that the surface of the iron oxide clusters is covered with a layer of N-doped carbon, indicating that the carbon nitride formed by the decomposition of melamine during pyrolysis effectively isolates the iron nanoclusters and prevents the agglomeration of iron.[1] The dark-field scanning transmission electron microscopy images of $Fe_3N_{1.5}C$ (Figure S4b) further illustrate the dispersion of iron oxide nanoparticles on NCNT. The energy dispersive X-ray (EDS) mapping image (Figure S4c) shows that N and O elements are evenly distributed in the entire carbon skeleton, and Fe element mainly exists in the form of nanoparticle aggregates.

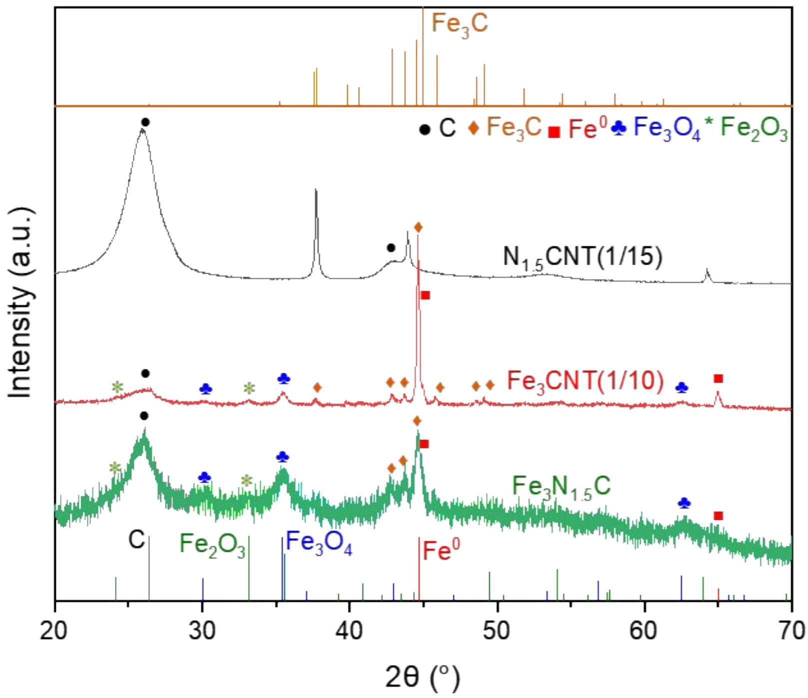

Figure S5 XRD patterns of $Fe_3N_{1.5}C$, Fe_3CNT (1/10 of the actual signal value) and $N_{1.5}CNT$ (1/15 of the actual signal value).

The XRD patterns of the $Fe_3N_{1.5}C$, Fe_3CNT and $N_{1.5}CNT$ catalysts are shown in Figure S5. All three catalysts have a broad peak at about 26 °, which corresponds to the (002) crystal plane of graphite carbon. There are several peaks in the XRD spectra of Fe_3CNT, of which 44.7 ° and 65 ° belong to Fe^0 species, 45 °, 43.8 °, 42.9 ° and related peaks belong to Fe_3C species, 35.4 ° and 29.6 ° belong to Fe_3O_4 species, 33.2 ° and 35.6 ° belong to Fe_2O_3 species[2]. The XRD spectra of $Fe_3N_{1.5}C$ also found the same iron species as Fe_3CNT spectra. It is worth noting that the peak intensity corresponding to each species in the XRD pattern of $Fe_3N_{1.5}C$ is greatly weakened, indicating that the iron species are well dispersed in $Fe_3N_{1.5}C$, further indicating that N doping can effectively anchor the Fe species.

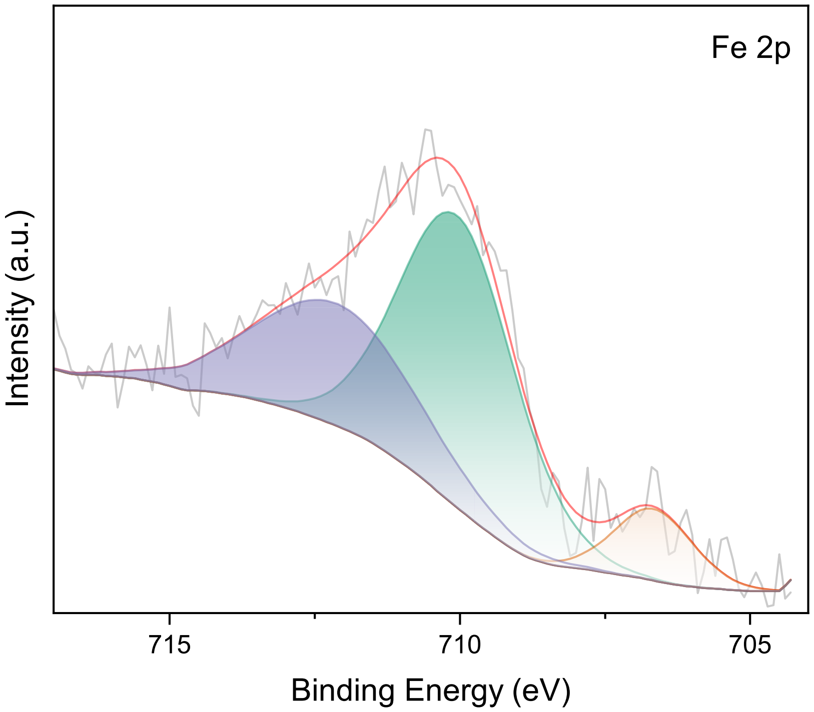

Figure S6 Fe 2p XPS spectra of the $Fe_3N_{1.5}C$ catalyst.

In the Fe 2p XPS spectra (Figure. S5) of the catalyst, the peaks near 706.7 eV, 710 eV and 712.1 eV can be attributed to Fe^0, Fe^{2+} and Fe^{3+}, respectively, confirming the existence of the Fe^0, Fe_3O_4 and Fe_2O_3.

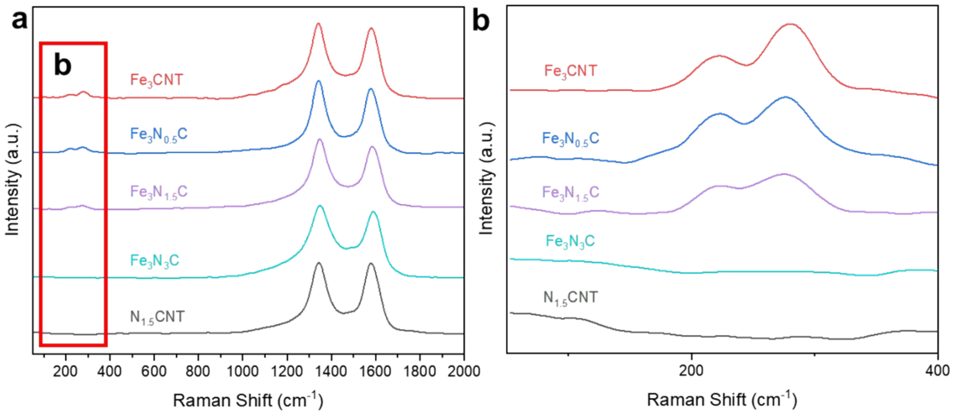

Figure S7 Raman shift of Fe$_3$N$_y$C, Fe$_3$CNT and N$_{1.5}$CNT.

The Raman spectrum (Figure S7a) of Fe$_3$N$_y$C, Fe$_3$CNT and N$_{1.5}$CNT catalysts show two obvious peaks at approximately 1,344 and 1,580 cm^{-1}, which are assigned to disorder (D) bands and graphitic (G) bands of sp2 carbon materials. The intensity ratio of D and G bands (I_D / I_G) is usually used as a descriptor to reflect the degree of defects and disorder[3]. With the increase of N doping amount, the I_D / I_G value decreases, that is, the degree of graphitization of the catalyst decreases, while the performance change trend of the catalyst is opposite, indicating that the degree of graphitization has little effect on the performance of the catalyst. It is worth noting that in the Raman spectrum of Fe$_3$CNT (Figure S7b), two peaks appear at 222 cm^{-1} and 282 cm^{-1}, corresponding to iron nanoclusters[4]. The peaks of iron nanoclusters appear in Fe$_3$N$_{0.5}$C and Fe$_3$N$_{1.5}$C after N doping, and the peaks of iron nanoclusters disappear with the further increase of N doping amount. It shows that with the increase of N doping amount, the iron nanoclusters gradually decrease until the characteristic peak disappears on the Raman spectrum, which confirms the anchoring effect of N doping on iron.

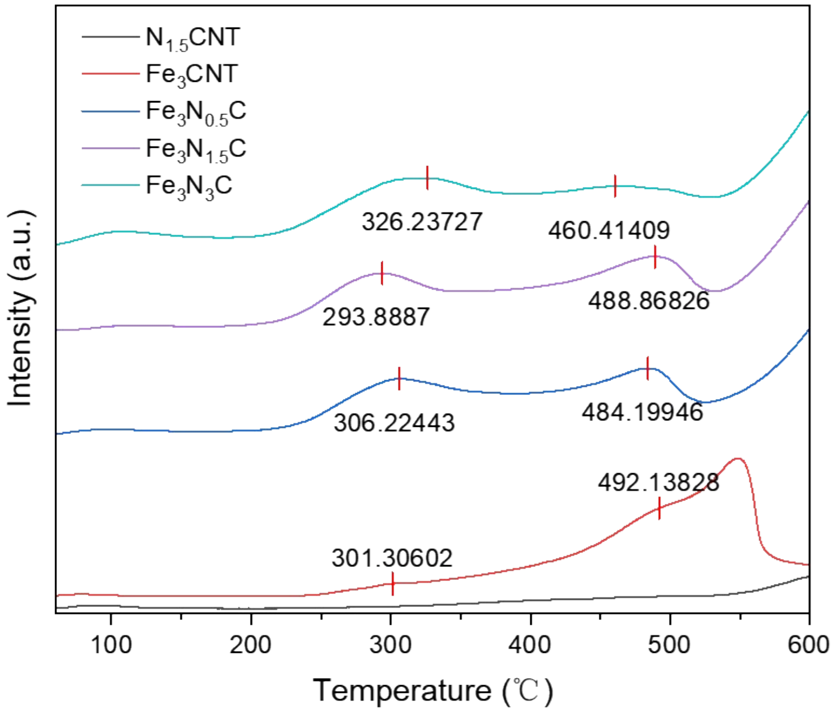

Figure S8 H_2-TPR spectra of Fe_3N_yC, Fe_3CNT and $N_{1.5}CNT$.

Figure S8 illustrates that the Fe_3CNT catalyst exhibits two peaks of H_2 consumption before 500°C, attributed to the reduction of $Fe_3O_4 \rightarrow FeO$ (around 300°C) and $FeO \rightarrow Fe^0$ (around 480 °C)[5] .Indeed, these two peaks were also observed in $Fe_3N_{0.5}C$ after N doping, with the peak at 300°C being significantly enhanced while the peak at 480 °C was slightly reduced. This observation suggests that the doping of N enhances the reducibility of Fe oxide at low temperatures. Furthermore, as the N doping amount increases, the reduction peak corresponding to 300 °C initially shifts towards lower temperatures and then towards higher temperatures after the N doping ratio reaches 1.5. This phenomenon indicates that increasing N doping can enhance the reducibility of iron oxides at low temperatures, but the effect diminishes after exceeding a certain amount, consistent with the SCR performance test results of the catalyst[3].

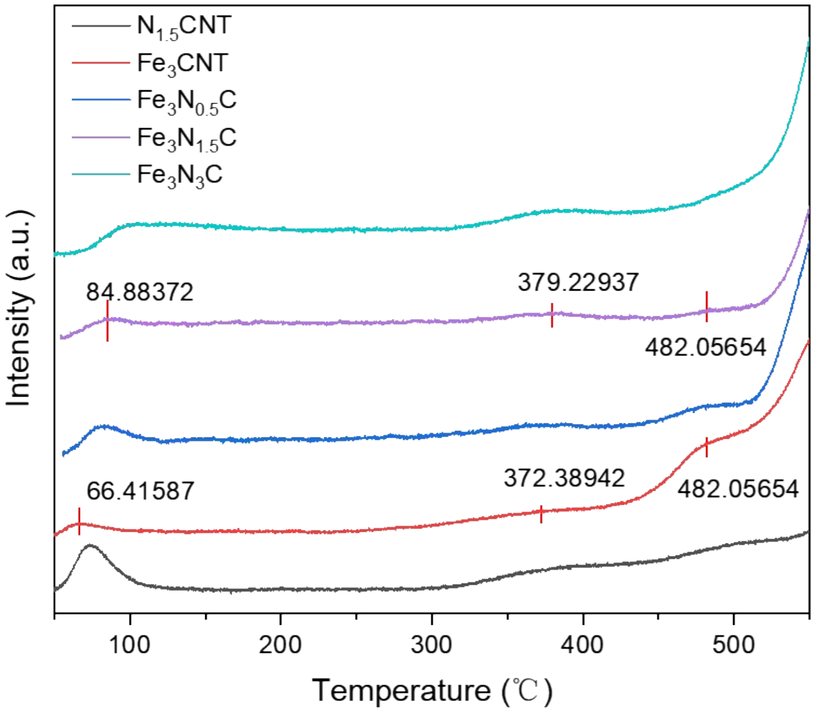

Figure S9 NH_3-TPD spectra of Fe_3N_yC, Fe_3CNT and $N_{1.5}CNT$

Figure S9 presents the NH_3-TPD results of Fe_3N_yC, Fe_3CNT, and $N_{1.5}CNT$ catalysts, revealing similar TPD profiles in the temperature range of 50-550°C, indicating the presence of the same acid site distribution. Each catalyst exhibits three peaks: the peak at 50-100°C represents physically adsorbed NH_3, the peak at 300-400°C belongs to moderate acid sites, and the peak above 400°C belongs to strong acid sites[6]. None of the catalysts show peaks corresponding to weak acid sites in the range of 100-200°C. Relative to Fe_3CNT, the peak value of Fe_3N_yC catalyst at 50-100°C increased, while the peak value of medium-strong acid sites at 300-400°C did not change significantly, and the peak value of strong acid sites above 400°C decreased to some extent. This indicates that the incorporation of N precursors enhances the physical adsorption capacity of the catalyst but covers strong acid sites to a certain extent. This finding contradicts the effect of N doping on the catalyst's performance, suggesting that the number of strong acid sites has minimal impact on the catalyst's performance.

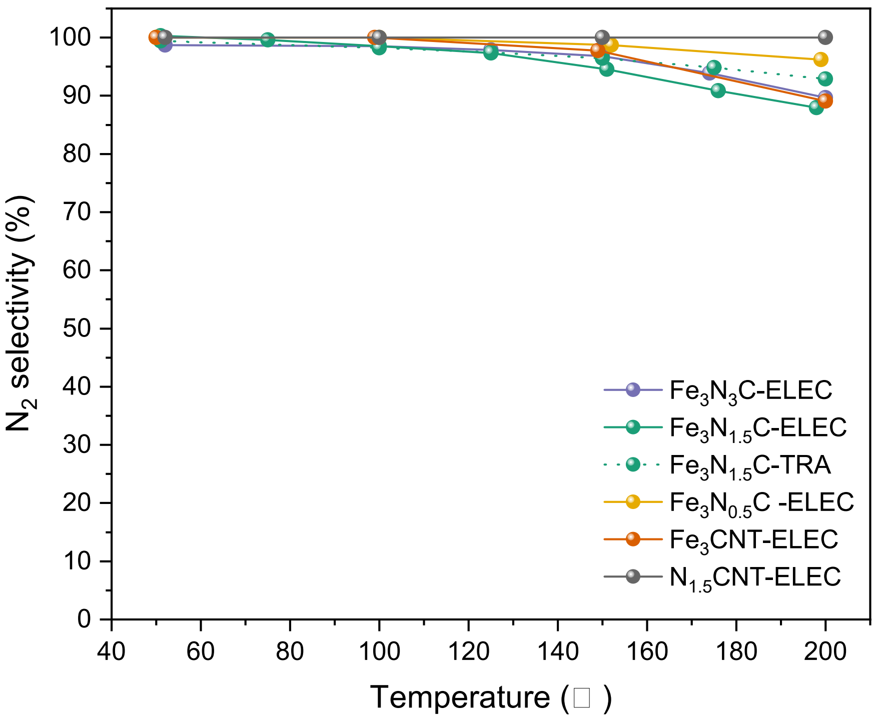

Figure S10 N_2 selectivity of the catalyst under TRA and ELEC.

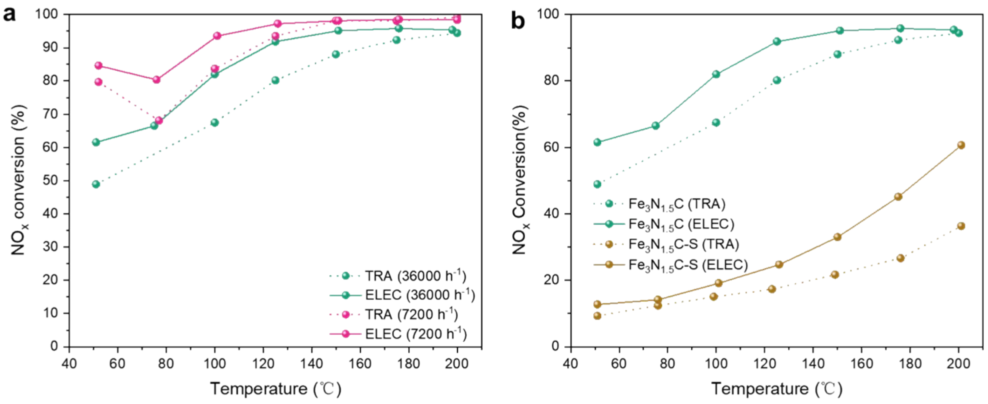

Figure S11 NO$_x$ conversion of Fe$_3$N$_{1.5}$C under TRA and ELEC (a) at different space velocities, (b) before and after SO$_2$ poisoning (200ppm SO$_2$ and 10% H$_2$O for 10h).

In order to analyze the anti-sulfur effect of ELEC, sulfur dioxide poisoning samples were prepared in this study. Initially, the Fe$_3$N$_{1.5}$C catalyst was poisoned in 10% water and 200 ppm SO$_2$ for 10 hours, followed by testing of NH$_3$-SCR performance under ELEC and TRA conditions. As illustrated in Fig. S11b, both ELEC and TRA performances of Fe$_3$N$_{1.5}$C experienced a significant decrease after sulfur poisoning, with the ELEC performance notably surpassing the TRA performance. Specifically, at 200°C, the ELEC performance exceeded that of TRA by a considerable margin. While the ELEC performance reached 60%, the TRA performance lagged behind at only 36%. This outcome underscores that ELEC helps to mitigate the adverse effects of sulfur poisoning on catalyst performance, consistent with existing research findings[7]. Previous studies by Li et al. [8] suggest that the enhanced sulfur resistance observed under electrically assisted conditions may be attributed to the facilitated decomposition of surface-deposited NH$_4$HSO$_4$ species. This electrochemical decomposition process effectively mitigates sulfur poisoning by preventing the accumulation of deactivating sulfate species on the catalyst surface.

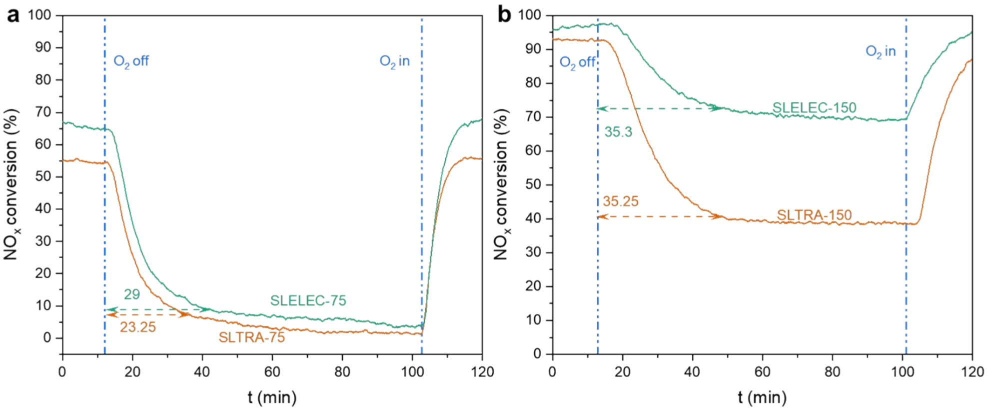

Figure S12 O_2 on−off experiments of $Fe_3N_{1.5}C$ catalyst under TRA and ELEC at 75 °C (a) and 150 °C (b).

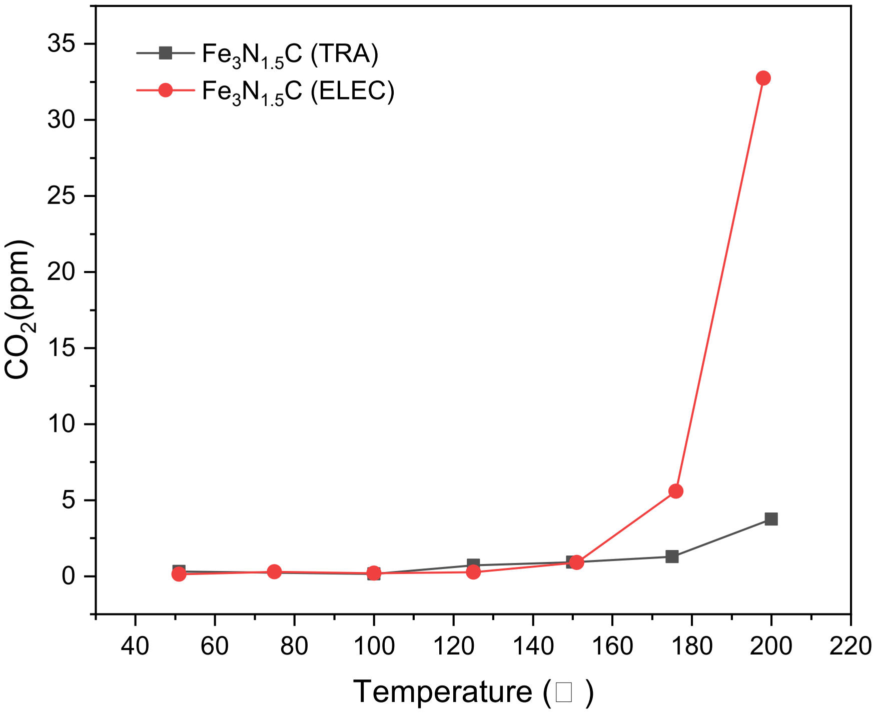

Figure S13 CO_2 production of $Fe_3N_{1.5}C$ under TRA and ELEC

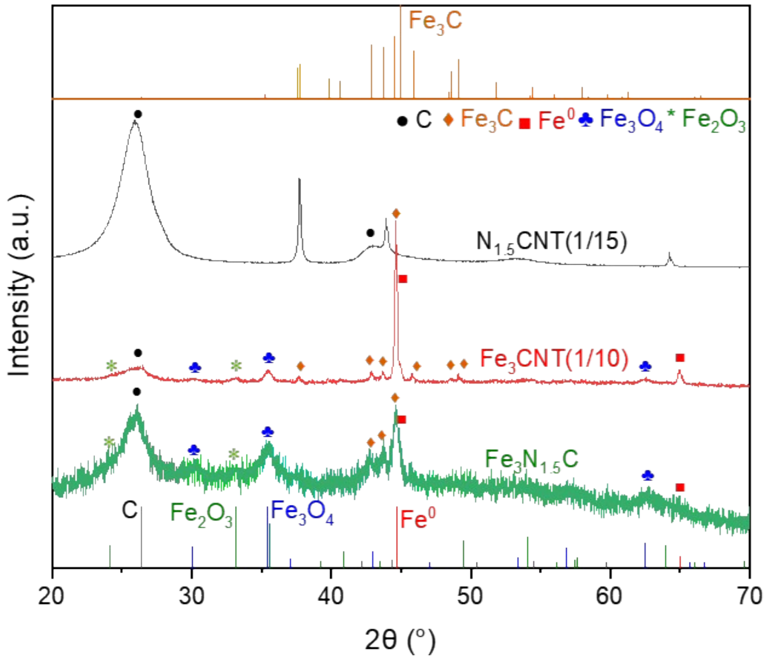

Figure S14 XRD spectra of Fe_3N_yC, Fe_3CNT and $N_{1.5}CNT$.

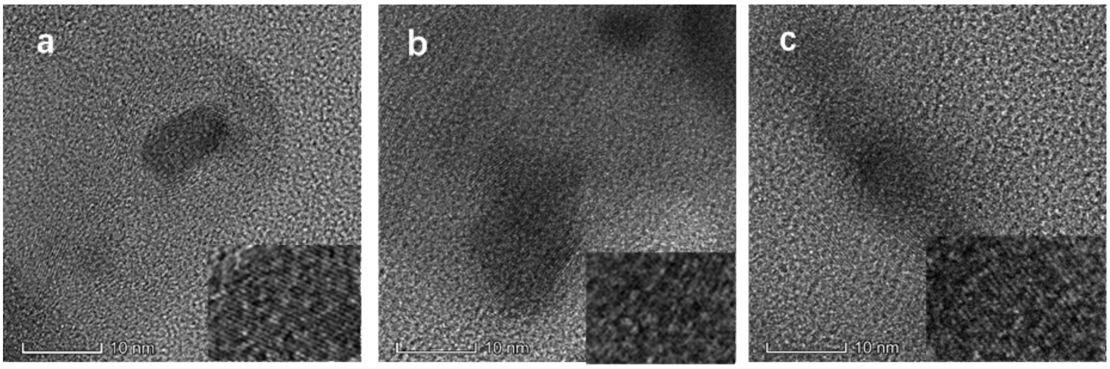

Figure S15 HRTEM images of (a) fresh Fe3N1.5C catalyst, (b) Fe3N1.5C catalyst following OF-ELEC, and (c) Fe3N1.5C catalyst following OF-ELEC repeat.

References

[1] K. Qian, H. Chen, W. Li, Z. Ao, Y.-n. Wu, X. Guan, Single-Atom Fe Catalyst Outperforms Its Homogeneous Counterpart for Activating Peroxymonosulfate to Achieve Effective Degradation of Organic Contaminants, Environmental Science & Technology, 55 (2021) 7034-7043.
[2] R. Hao, S. Fang, L. Tian, R. Xia, Q. Guan, L. Jiao, Y. Liu, W. Li, Elucidation of the electrocatalytic activity origin of Fe3C species and application in the NOx full conversion to valuable ammonia, Chemical Engineering Journal, 467 (2023) 143371.
[3] Q. Zhao, S. Huang, X. Han, J. Chen, J. Wang, A. Rykov, Y. Wang, M. Wang, J. Lv, X. Ma, Highly active and controllable MOF-derived carbon nanosheets supported iron catalysts for Fischer-Tropsch synthesis, Carbon, 173 (2021) 364-375.
[4] A. Halepoto, M. Kashif, Y. Su, J. Cheng, W. Deng, B. Zhao, Preparations and Characterization on Fe Based Catalyst Supported on Coconut Shell Activated Carbon CS(AC) and SCR of NOx-HC, Catalysis Surveys from Asia, 24 (2020) 123-133.
[5] B. Gu, S. He, W. Zhou, J. Kang, K. Cheng, Q. Zhang, Y. Wang, Polyaniline-supported iron catalyst for selective synthesis of lower olefins from syngas, Journal of Energy Chemistry, 26 (2017) 608-615.
[6] J.-R. Youn, M.-J. Kim, S.-J. Lee, I.-S. Ryu, S.K. Jeong, K. Lee, S.G. Jeon, The effect of CNTs on V-Ce/TiO2 for low-temperature selective catalytic reduction of NO, Korean Journal of Chemical Engineering, 39 (2022) 2334-2344.
[7] L. Dou, C. Yan, L. Zhong, D. Zhang, J. Zhang, X. Li, L. Xiao, Enhancing CO2 methanation over a metal foam structured catalyst by electric internal heating, Chemical Communications, 56 (2020) 205-208.
[8] W. Li, X. Du, Z. Li, Y. Tao, J. Xue, Y. Chen, Z. Yang, J. Ran, V. Rac, V. Rakić, Electrothermal alloy embedded V2O5-WO3/TiO2 catalyst for NH3-SCR with promising wide operating temperature window, Process Safety and Environmental Protection, 159 (2022) 213-220.